Dynamic actin filaments control the mechanical behavior of the human red blood cell membrane

David S. Gokhin[a], Roberta B. Nowak[a], Joseph A. Khoory[b], Alfonso de la Piedra[b], Ionita C. Ghiran[b], and Velia M. Fowler[a]

[a]Department of Cell and Molecular Biology, The Scripps Research Institute, La Jolla, CA 92037; [b]Department of Medicine, Beth Israel Deaconess Medical Center, Boston, MA 02115

ABSTRACT Short, uniform-length actin filaments function as structural nodes in the spectrin-actin membrane skeleton to optimize the biomechanical properties of red blood cells (RBCs). Despite the widespread assumption that RBC actin filaments are not dynamic (i.e., do not exchange subunits with G-actin in the cytosol), this assumption has never been rigorously tested. Here we show that a subpopulation of human RBC actin filaments is indeed dynamic, based on rhodamine-actin incorporation into filaments in resealed ghosts and fluorescence recovery after photobleaching (FRAP) analysis of actin filament mobility in intact RBCs (~25–30% of total filaments). Cytochalasin-D inhibition of barbed-end exchange reduces rhodamine-actin incorporation and partially attenuates FRAP recovery, indicating functional interaction between actin subunit turnover at the single-filament level and mobility at the membrane-skeleton level. Moreover, perturbation of RBC actin filament assembly/disassembly with latrunculin-A or jasplakinolide induces an approximately twofold increase or ~60% decrease, respectively, in soluble actin, resulting in altered membrane deformability, as determined by alterations in RBC transit time in a microfluidic channel assay, as well as by abnormalities in spontaneous membrane oscillations (flickering). These experiments identify a heretofore-unrecognized but functionally important subpopulation of RBC actin filaments, whose properties and architecture directly control the biomechanical properties of the RBC membrane.

INTRODUCTION

The mammalian red blood cell (RBC) is structurally unique in that it contains no nucleus, intracellular organelles, or transcellular cytoskeleton. Underlying the RBC plasma membrane is the membrane skeleton, a two-dimensional isotropic cytoskeletal network with quasi-hexagonal symmetry. The membrane skeleton consists of nodes of short (~37-nm-long) actin filaments interconnected by long strands of $(\alpha_1\beta_1)_2$-spectrin tetramers (Fowler, 2013). The actin filaments of the RBC membrane skeleton are each attached to five to seven $(\alpha_1\beta_1)_2$-spectrin tetramers stabilized along their lengths by two tropomyosin isoforms, TM5b (Tpm1.9) and TM5NM1 (Tpm3.1), capped at their pointed and barbed ends by tropomodulin1 (Tmod1) and $\alpha\beta$-adducin, respectively, and possibly bundled by dematin (functions reviewed in Fowler, 2013). Current models of the spectrin-actin membrane skeleton presume that the actin filaments function as stable nodes or linkages, whose subunits do not dynamically assemble or disassemble (Fowler, 2013). The RBC membrane skeleton is the prototypical membrane-associated cytoskeleton, serving as a platform for understanding the assembly and maintenance of specialized membrane protein domains in diverse cell types, such as the transverse tubules and intercalated disks of cardiomyocytes, costameres of skeletal muscle fibers, axon initial segments and nodes of Ranvier in neurons, and lateral membrane domains of polarized epithelial cells (Bennett and Gilligan, 1993; Bennett and Baines, 2001; Bennett and Lorenzo, 2013). Therefore, understanding the

basis for membrane skeleton assembly, stability, and connectivity is of broad biological importance.

Several studies have indicated that the architecture of RBC actin filament nodes mediates the connectivity of the membrane skeleton and imparts the RBC with the biconcave shape and biomechanical properties optimized for efficient passage through the microvasculature. RBC actin filament uncapping via targeted genetic deletion of Tmod1 or the α or β subunit of adducin in mice leads to abnormal RBC shapes (spheroelliptocytosis), with increased osmotic fragility and reduced deformability, resulting in hemolytic anemias of varying severities (Gilligan et al., 1999; Muro et al., 2000; Porro et al., 2004; Chen et al., 2007; Robledo et al., 2008; Moyer et al., 2010). Furthermore, simultaneous deletion of β-adducin and the dematin headpiece domain required for actin bundling results in more-pronounced spherocytosis and a correspondingly more-severe anemia (Chen et al., 2007; Liu et al., 2011). In the case of Tmod1 deletion, the short actin filaments in the membrane skeleton become more variable in length (Moyer et al., 2010), implying altered actin assembly/disassembly, although this has not been directly demonstrated. Moreover, actin filament assembly in the RBC membrane skeleton has been implicated in the origin of RBC membrane "flickering" (i.e., spontaneous and ATP-dependent vibrational oscillations of the RBC membrane; Burton et al., 1968; Levin and Korenstein, 1991; Tuvia et al., 1992, 1998; Costa et al., 2008; Betz et al., 2009; Yoon et al., 2009). This has been supported by experimental observations of reduced flickering after chemical inhibition of actin filament barbed-end assembly (Tuvia et al., 1998).

The uniform lengths of the short RBC actin filaments and their locations at nodes of the spectrin-actin membrane skeleton have led to the current assumption that RBC actin filaments are not dynamic (i.e., do not exchange subunits with G-actin in the cytosol during normal RBC homeostasis). However, whether RBC actin filaments might be dynamic and, if so, whether actin dynamics regulates membrane skeleton connectivity and/or RBC mechanical properties are questions that have never been rigorously addressed. Several lines of evidence have hinted, but not directly proven, that a dynamic process of actin subunit turnover may occur in RBCs. First, the RBC cytosol contains ~10 µg/ml (0.24 µM) G-actin, which is slightly greater than the barbed-end critical concentration (Pinder and Gratzer, 1983; Pollard et al., 2000), suggesting that soluble actin subunits may exchange with subunits at the barbed ends. Consistent with this, a cytosolic actin population has been visualized via immunogold labeling of sections of intact RBCs (Cyrklaff et al., 2011). Second, it has been shown that infection of human RBCs with the malaria-causing parasite *Plasmodium falciparum* results in dramatic remodeling of RBC actin filaments into an aberrantly branched network in the cytosol to facilitate export of virulence factors (Cyrklaff et al., 2011; Rug et al., 2014). Presumably, such reorganization requires dynamic disassembly/reassembly of actin filaments.

Here, we directly probed the mechanisms of actin dynamics in RBCs via treatment with the actin-disrupting drugs cytochalasin-D (CytoD), latrunculin-A (LatA), and jasplakinolide (Jasp). CytoD inhibits actin subunit association and dissociation at barbed ends; LatA destabilizes and depolymerizes dynamic actin filaments by binding to and sequestering actin monomers, driving the F:G-actin balance toward the G-actin state; and Jasp stabilizes dynamic actin filaments, driving the F:G-actin balance toward the F-actin state (MacLean-Fletcher and Pollard, 1980; Cooper, 1987; Coue et al., 1987; Spector et al., 1989; Sampath and Pollard, 1991; Bubb et al., 1994, 2000; Morton et al., 2000; Allingham et al., 2006; Holzinger, 2009). Our results show that rhodamine-actin (rho-actin) subunits incorporate into discrete sites within the membrane skeleton in resealed RBC ghosts, suggesting that a subpopulation of RBC actin filaments is indeed available for subunit exchange. Rho-actin subunit incorporation can be blocked via treatment with CytoD, demonstrating that subunit exchange occurs at barbed ends. Moreover, fluorescence recovery after photobleaching (FRAP) analysis revealed a mobile subpopulation of RBC actin filaments (~25–30% of total actin filaments), whose mobility can be partially attenuated via treatment with CytoD. Consistent with subunit assembly/disassembly, treatment with LatA or Jasp induces an approximately twofold increase or ~60% decrease, respectively, in soluble actin. Neither LatA nor Jasp treatment affected RBC osmotic fragility, but both LatA and Jasp treatment resulted in altered membrane deformability and flickering. Collectively, these results provide the first direct evidence for the existence of a dynamic and mobile RBC actin filament subpopulation and that actin filament architecture directly controls the mechanics of the human RBC membrane.

RESULTS

Characterization of RBC actin subunit exchange and filament mobility

A previous study measured a G-actin concentration of ~0.24 µM in human RBC cytosol, based on the ability of G-actin to inhibit DNase I activity (Pinder and Gratzer, 1983). We reinvestigated the concentration of cytosolic G-actin in RBCs by using Western blots to compare the relative proportions of actin in Triton X-100–extracted membrane skeletons versus RBC cytosolic fractions. This experiment revealed that ~96.3% of human RBC actin is membrane skeleton associated, whereas ~3.7% is cytosolic (Figure 1, A and B), similar to our previous analyses of mouse RBC actin (Moyer et al., 2010). This distribution of insoluble versus cytosolic actin is comparable to the distribution observed in mouse skeletal muscle, in which ~5–10% of total actin is cytosolic (Gokhin and Fowler, 2011), but differs markedly from cell types with rapidly remodeling actin cytoskeletons, such as migrating vascular endothelial cells, in which ~50–60% of total actin is cytosolic (Hinshaw et al., 1993; Fischer et al., 2003). Assuming ~500,000 actin subunits in the human RBC membrane skeleton (Pinder and Gratzer, 1983; Fowler, 1996) and a typical human RBC volume of 90 fl (Kaushansky et al., 2010), we calculate a total (membrane skeleton–associated plus cytosolic) actin concentration of ~9.6 µM in RBCs (Figure 1B). Moreover, assuming that RBCs do not contain G-actin–sequestering proteins, our data reveal a cytosolic G-actin concentration of ~0.36 µM (Figure 1B), which is ~50% greater than the value of ~0.24 µM reported previously (Pinder and Gratzer, 1983) and halfway between the actin barbed-end and pointed-end critical concentrations of 0.1 and 0.6 µM, respectively (Pollard et al., 2000).

Next, to directly address whether dynamic actin subunit assembly or exchange occurs between the RBC membrane skeleton and cytosol, we resealed human RBC ghosts in the presence of rho-actin for 30 min and then visualized rho-actin incorporation. In dimethyl sulfoxide (DMSO)–treated ghosts, rho-actin localized to discrete sites around the RBC circumference, consistent with dynamic incorporation of rho-actin subunits into the membrane skeleton (Figure 1C). This effect was dramatically attenuated in ghosts treated with 0.5 µM CytoD to inhibit barbed-end exchange (Figure 1C), indicating that barbed-end exchange mediates rho-actin incorporation into the RBC membrane skeleton, consistent with a cytosolic G-actin concentration of ~0.36 µM (Figure 1B). However, the discrete foci of rho-actin incorporation suggest that only a subpopulation of actin filaments is available for barbed-end incorporation within the experiment's 30-min time frame. We confirmed CytoD
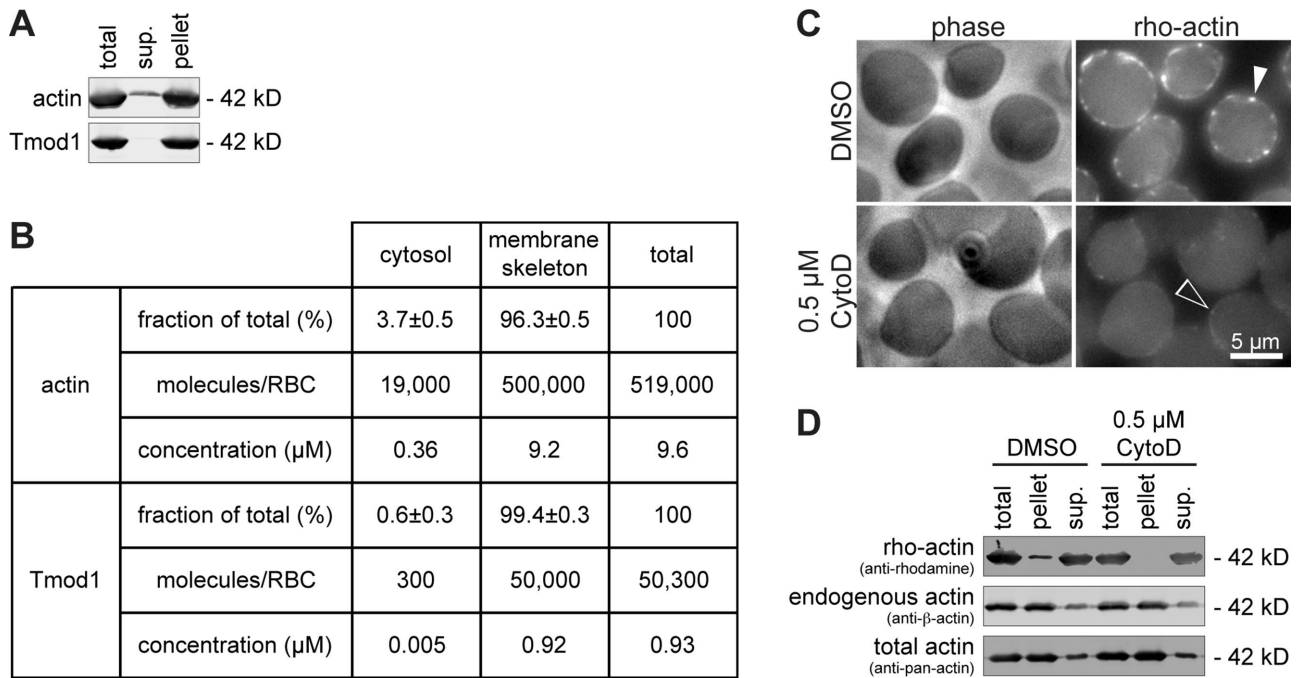
FIGURE 1: Inhibition of barbed-end exchange with CytoD blocks dynamic incorporation of rho-actin subunits into the RBC membrane skeleton. (A) Western blots for actin and Tmod1 in total human RBC extracts, RBC cytosolic fractions (supernatants), and Triton X-100–extracted membrane skeletons (pellets). (B) Tabulation of actin and Tmod1 stoichiometry in RBCs. Note that ~96.3% of actin and, for comparison, virtually all Tmod1 is associated with the membrane skeleton. Cytosolic and total actin molecules per RBC were based on a value of 500,000 actin subunits/ membrane skeleton (Pinder et al., 1981; Pinder and Gratzer, 1983), and actin concentrations were based on an average human RBC volume of 90 fl (Kaushansky et al., 2010). (C) Phase-contrast (left) and fluorescence (right) micrographs of human RBC ghosts incubated in 2.4 µM rho-actin and either DMSO (top) or 0.5 µM CytoD (bottom) for 10 min on ice and then resealed and incubated for 30 min at 37°C. In DMSO-treated ghosts, rho-actin localizes to bright puncta along the ghost membrane (white arrowhead), indicating incorporation into the membrane skeleton. In CytoD-treated ghosts, incorporation of rho-actin into the membrane skeleton is markedly reduced, as indicated by fewer and fainter rho-actin puncta (black arrowhead). (D) Western blots of human RBC ghosts incubated in 2.4 µM rho-actin and either DMSO or 0.5 µM CytoD for 10 min on ice and then resealed and incubated for 30 min at 37°C. Ghosts were then extracted by Triton X-100 and centrifuged to obtain cytosolic fractions (supernatants) and Triton X-100–extracted membrane skeletons (pellets). Western blotting was performed using an anti-rhodamine antibody to assess distribution of exogenous rho-actin (top), an anti–β-actin antibody to assess distribution of endogenous RBC actin (exclusively β-actin; Pinder and Gratzer, 1983); middle), and an anti–pan-actin antibody to assess distribution of total actin (exogenous rho-actin plus endogenous RBC actin; bottom).

inhibition of rho-actin incorporation into the membrane skeleton by Western blotting of Triton X-100–extracted membrane skeletons versus cytosolic fractions using an anti-rhodamine antibody (Figure 1D). Additional evidence in favor of dynamic subunit exchange comes from our observation that a small amount of endogenous RBC actin is displaced from the membrane skeleton fraction to the cytosolic fraction in the presence of rho-actin (compare Figure 1, A and D), as determined by Western blotting using an antibody against β-actin, the singular endogenous actin isoform in RBCs (Pinder and Gratzer, 1983).

To determine whether inhibition of barbed-end exchange might also influence overall RBC actin filament stability, we incubated intact RBCs with increasing concentrations of CytoD and performed Western blots to detect changes in soluble actin. We observed no changes in the amount of soluble actin in RBCs treated with CytoD concentrations up to 1 µM (Figure 2, A and D), indicating that inhibition of barbed-end exchange does not lead to net assembly or disassembly of RBC actin filaments. This finding was supported by Alexa 488–phalloidin staining and total internal reflection fluorescence (TIRF) microscopy of CytoD-treated RBCs, which showed diffuse

and uniform F-actin staining across the RBC membrane, indistinguishable from DMSO-treated RBCs (Figure 2G). We conclude that the incorporation of rho-actin into discrete foci in the membrane skeleton is likely due to rho-actin subunit exchange with actin subunits at barbed ends of a subpopulation of the endogenous actin filaments in the membrane skeleton.

Although our rho-actin incorporation experiments indicate turnover of at least some individual RBC actin filaments, an alternative approach is required to determine the fraction of actin filaments that are mobile in intact RBCs. To study this question, we labeled the actin filaments in the membrane skeleton of intact living RBCs with a cell-permeable infrared-fluorescent Jasp conjugate, silicon-rhodamine (SiR)-Jasp, which was developed to study actin mobility in living cells and previously referred to as SiR-actin (Lukinavicius et al., 2014). SiR-Jasp is particularly advantageous for investigations of RBCs due to the nonoverlap of the emission spectrum of SiR with the absorption spectrum of hemoglobin (Lukinavicius et al., 2014). As expected, SiR-Jasp efficiently labeled RBC actin filaments, based on bright rim staining visualized by wide-field fluorescence microscopy (Figure 3A). SiR-Jasp was also confirmed to selectively label
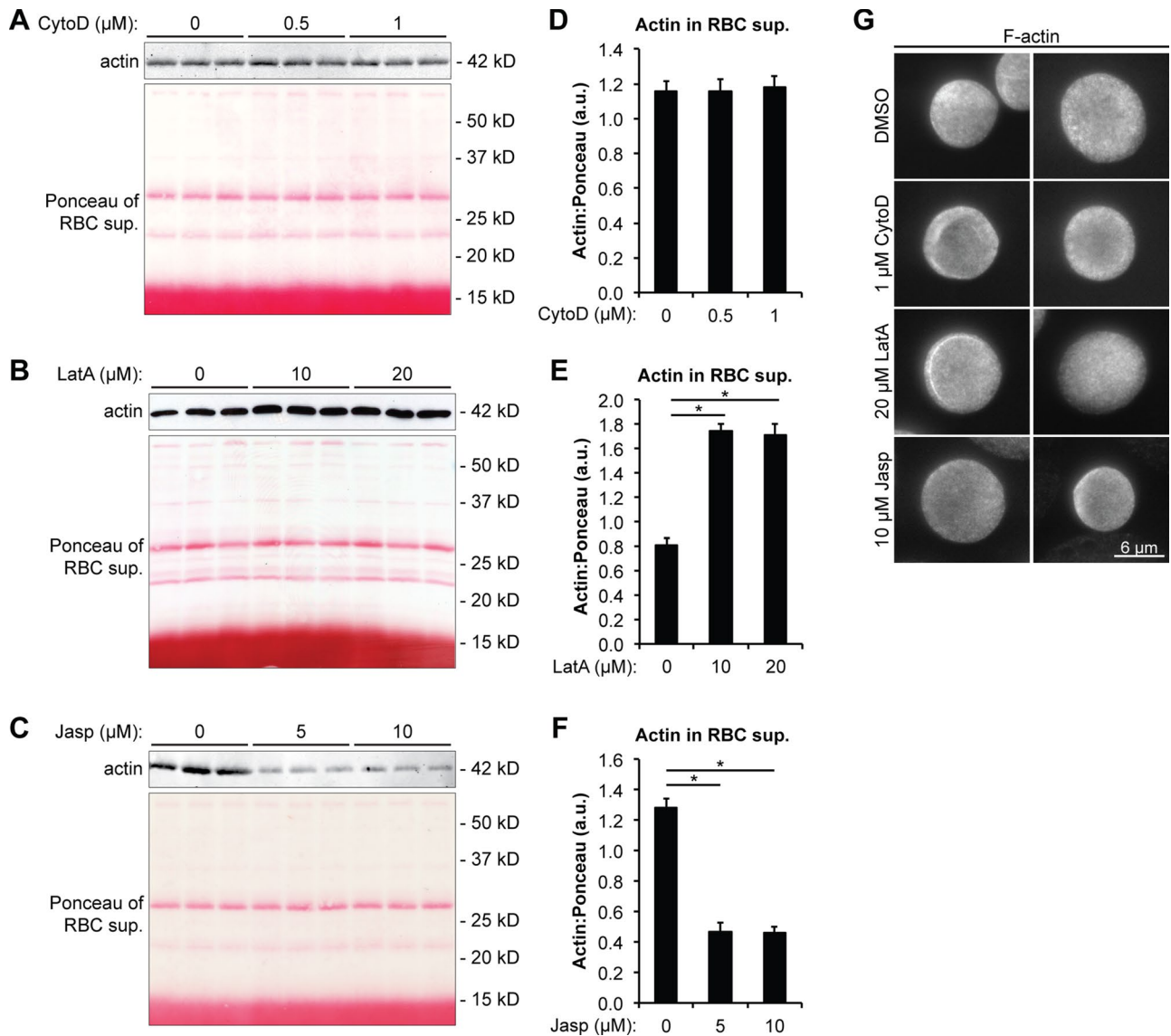
FIGURE 2: Treatment with LatA and Jasp (but not CytoD) alters the soluble actin pool in human RBCs without affecting the diffuse localization pattern of F-actin determined by TIRF microscopy. (A–C) Western blots of Triton X-100–extracted supernatants prepared from intact RBCs treated with the indicated concentrations of (A) CytoD, (B) LatA, or (C) Jasp and then lysed with Triton-lysis buffer. (D–F) Quantitation of Western blots in A–C. Note that CytoD has no effect on the soluble actin pool, 10 µM LatA results in approximately twofold increase in soluble actin that does not increase further with increasing concentrations of LatA, and 5 µM Jasp results in ~60% decrease in soluble actin that does not decrease further with increasing concentrations of Jasp. In all experiments, Ponceau S served as a loading control for normalization of actin levels. Error bars indicate mean ± SEM of $n = 3$ lanes. *$p < 0.01$. (G) Representative TIRF micrographs of RBCs stained with Alexa 488–phalloidin to label F-actin associated with the RBC membrane. Note the diffuse and uniform localization of F-actin in all drug treatment groups. Variability in RBC size and apparent "folds" in the RBC membrane are artifacts arising from cytocentrifugation onto glass slides.

the membrane skeleton by using TIRF microscopy (unpublished data), similar to Alexa 488–phalloidin staining of fixed and permeabilized RBCs imaged by TIRF microscopy (Figure 2G).

We performed FRAP analysis of intact, living SiR-Jasp–labeled RBCs by photobleaching a 1-µm-diameter spot, followed by collection of fluorescence images for at least 15 min (Figure 3B). After applying correction for nonspecific photobleaching arising from repetitive image acquisition, as described previously (Quadri et al., 2012; Melhorn et al., 2013), we found that recovery of SiR-Jasp fluorescence occurred within minutes. By applying exponential curve

fitting to the corrected fluorescence versus time traces (Reits and Neefjes, 2001), we calculated that an average of ~25–30% of the SiR-Jasp-labeled RBC actin filaments comprises a mobile subpopulation (Figure 3C). The observed fluorescence recovery was due to bona fide F-actin mobility and was not an artifact resulting from association/dissociation of the SiR-Jasp probe, because fixation in 0.5% acrolein before SiR-Jasp staining abolished fluorescence recovery and reduced the apparent mobile fraction of F-actin to almost 0% without affecting the SiR-Jasp labeling of the RBCs (Figure 3C). Intriguingly, inhibition of barbed-end exchange via
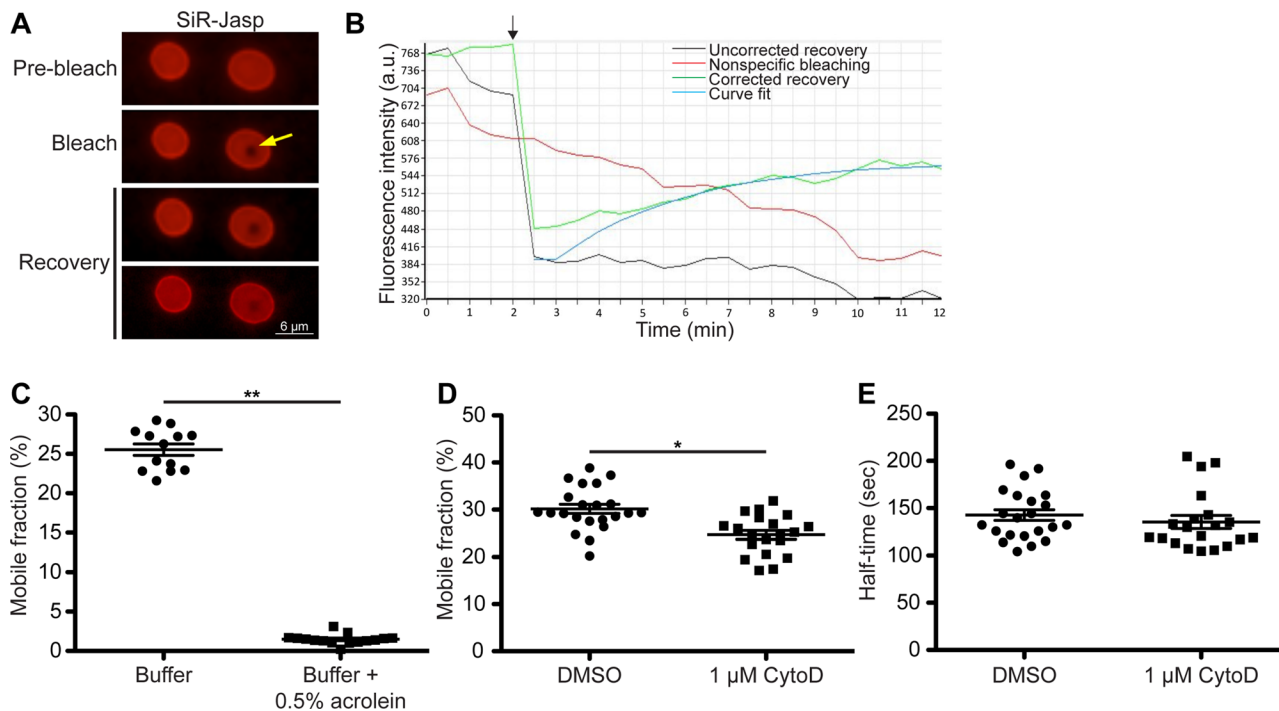
FIGURE 3: FRAP analysis of SiR-Jasp–stained human RBCs reveals F-actin mobility that can be reduced by CytoD treatment. (A) Example fluorescence micrographs of SiR-Jasp–stained RBCs before photobleaching, at the time of photobleaching, and during postphotobleaching recovery. Yellow arrow indicates photobleached area. (B) Example FRAP data. The black trace represents an original, uncorrected recovery curve measured in a photobleached area. The red trace represents nonspecific, off-target bleaching measured in same RBC but away from the photobleached area. The green trace represents the recovery curve corrected for nonspecific, off-target bleaching during repetitive image acquisition. The blue trace represents exponential curve fitting used to calculate F-actin mobile fraction and half-time of fluorescence recovery. Black arrow indicates the time of photobleaching. (C) Dotplot of F-actin mobile fraction in RBCs in buffer with or without fixation in 0.5% acrolein before SiR-Jasp staining. (D, E) Dotplots of (D) F-actin mobile fraction and (E) half-time of F-actin fluorescence recovery for RBCs treated with either DMSO or 1 μM CytoD. Each dot represents data from one RBC. $*p < 0.05$; $**p < 0.001$.

CytoD treatment slightly but significantly reduced the mobile fraction of RBC actin filaments (Figure 3D), although the half-time of fluorescence recovery was unaffected (Figure 3E), suggesting that barbed-end assembly partially accounts for actin filament mobility in RBCs. We conclude that approximately one-third of the filaments in the RBC actin filament network possess a heretofore-unrecognized capacity for forming new filaments, elongating existing filaments, undergoing micrometer-scale rearrangements, or a combination thereof. In addition, barbed-end actin subunit exchange at the single-filament level influences two-dimensional F-actin mobility in the plane of the membrane skeleton.

Treatment with LatA and Jasp perturbs RBC actin filament assembly

Treatment with LatA or Jasp provides a pharmacological means to alter F:G-actin balance for studying dynamic actin filament network function in living cells (for examples, see Ayscough et al., 1997; Wang et al., 2002, 2014; Pappas et al., 2010). As expected from LatA's monomer-sequestering function (Coue et al., 1987; Spector et al., 1989; Morton et al., 2000), LatA treatment of intact RBCs for 4 h led to an approximately twofold increase in soluble actin at a LatA concentration of 10 μM, and no additional increase in soluble actin was observed when the LatA concentration was raised to 20 μM (Figure 2, B and E). Similarly, as expected from Jasp's ability to stabilize actin filaments by inhibiting actin subunit dissociation from the

filaments (Bubb et al., 1994, 2000; Holzinger, 2009), Jasp treatment of intact RBCs for 4 h led to ~60% decrease in soluble actin at a Jasp concentration of 5 μM, and no additional decrease in soluble actin was observed when the Jasp concentration was raised to 10 μM (Figure 2, C and F). Because the overwhelming majority of RBC actin is associated with the insoluble membrane skeleton fraction (Figure 1, A and B), these changes in soluble actin do not result in concomitant decreases in insoluble actin of a sufficient magnitude to be detectable by Western blotting (unpublished data). The idea that the membrane skeleton remains grossly intact after drug treatment is supported by the observation that LatA treatment had no effect on the levels of soluble Tmod1, α-adducin, or TM5NM1 (Supplemental Figure S1) and that TIRF microscopy of LatA- and Jasp-treated RBCs found no changes in F-actin localization as compared with DMSO-treated RBCs (Figure 2G). Collectively, these data indicate that LatA or Jasp treatment provides a means to specifically perturb assembly/disassembly of a small subpopulation of RBC actin filaments.

Disruption of actin filament assembly/disassembly alters RBC membrane mechanics

To determine the role that actin filament assembly/disassembly might play in regulating RBC membrane mechanics, we subjected LatA- and Jasp-treated RBCs to a battery of functional assays. First, we observed that treatment with a LatA or Jasp concentration sufficiently high to disrupt RBC actin filaments (10 or 5 μM, respectively)
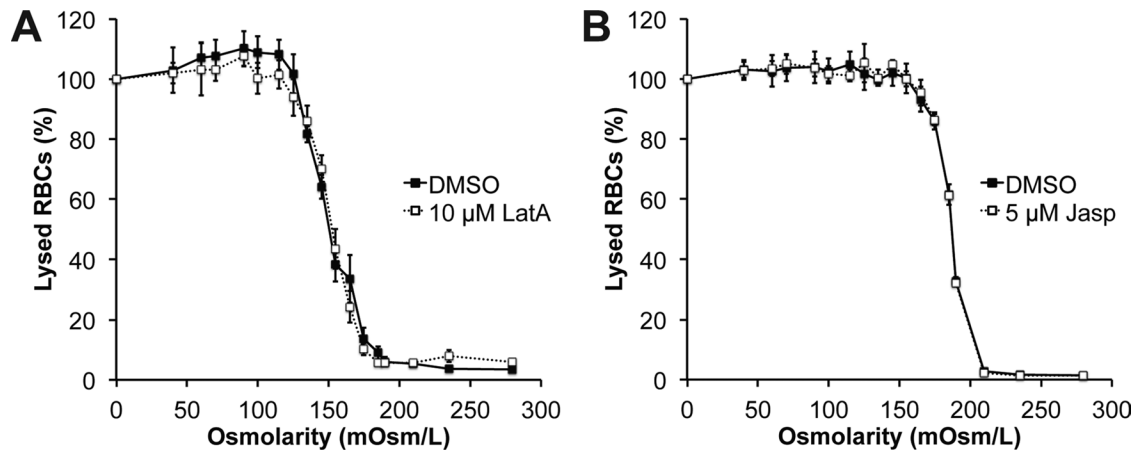
FIGURE 4: LatA or Jasp treatment does not affect the osmotic fragility of human RBCs. Curves depict the percentage of lysed RBCs as a function of buffer osmolarity for (A) RBCs treated with either DMSO or 10 μM LatA and (B) RBCs treated with either DMSO or 5 μM Jasp. Error bars indicate mean ± SEM of $n = 12$ replicates. Note that RBCs in A and B were obtained from different human donors and hence have somewhat different osmotic fragilities in the presence of DMSO alone.

had no effect on the osmotic fragility of RBCs (Figure 4). This indicates preserved membrane extensibility and ratio of surface area to volume (Mohandas and Chasis, 1993), which is consistent with the lack of discernible effects of LatA or Jasp on RBC sizes and shapes visualized by TIRF microscopy of Alexa 488-phalloidin–stained RBCs (Figure 3G). However, when we measured RBC transit times through 5-μm-wide microfluidic channels, mimicking RBC passage through capillaries (Shevkoplyas *et al.*, 2003, 2006; Ghiran *et al.*, 2011), we observed decreased transit times for both LatA- and Jasp-treated

RBCs (Figure 5), indicating enhanced membrane deformability. Enhanced membrane deformability was observed at 0.2 μM LatA and 0.5 μM Jasp, which are drug concentrations whose effects on RBC actin filament assembly/disassembly are not within the detection sensitivity of Western blotting for actin in RBC supernatants (compare Figure 2, A–F, and Supplemental Figure S2). Enhanced membrane deformability at such low drug concentrations highlights the remarkable sensitivity of RBC deformability to RBC actin filament assembly.
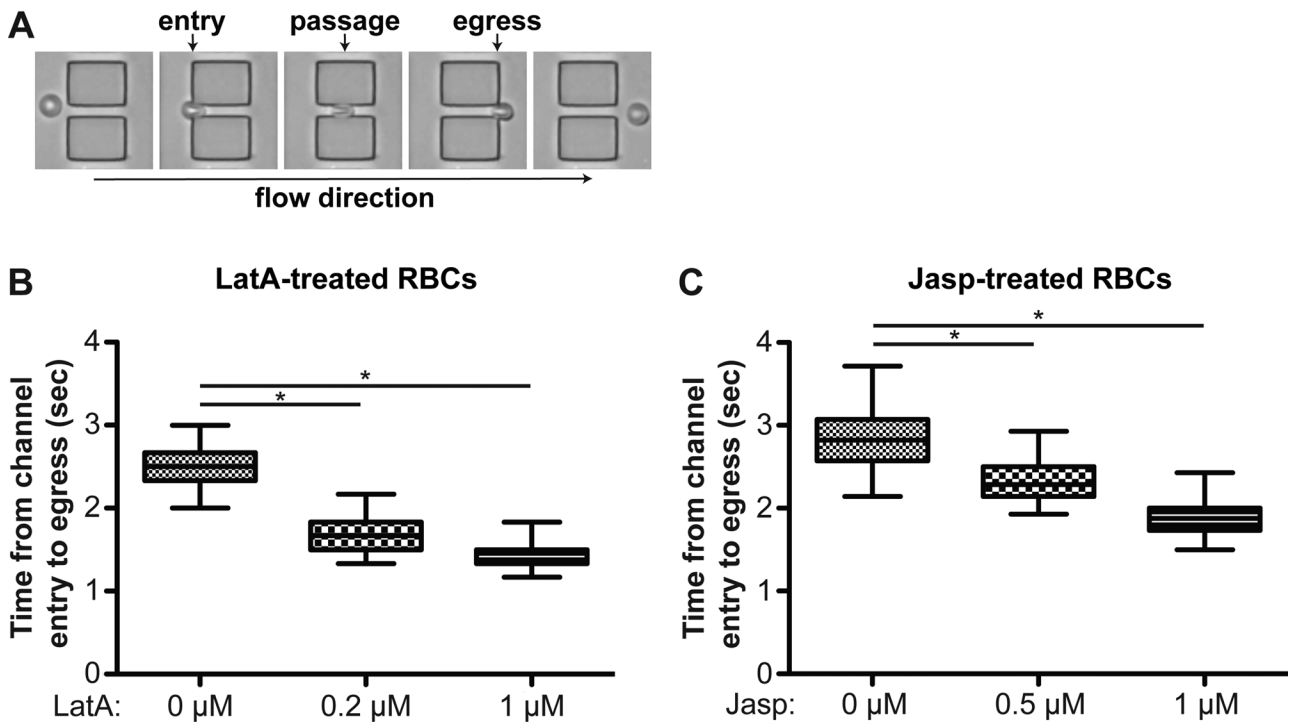

FIGURE 5: LatA or Jasp treatment increases the membrane deformability of human RBCs. (A) Representative video stills of RBC entry, passage, and egress through a microfluidic channel in response to fluid flow. (B, C) Boxplots depict RBC transit times through a microfluidic channel, from entry to egress, for RBCs treated with the indicated concentrations of (B) LatA or (C) Jasp. Decreased transit times of LatA- and Jasp-treated RBCs signify increased membrane deformability. Each boxplot reflects $n \geq 30$ RBCs. *$p < 0.01$. Note that RBCs in B and C were obtained from different human donors and hence have slightly different transit times in the presence of DMSO alone.
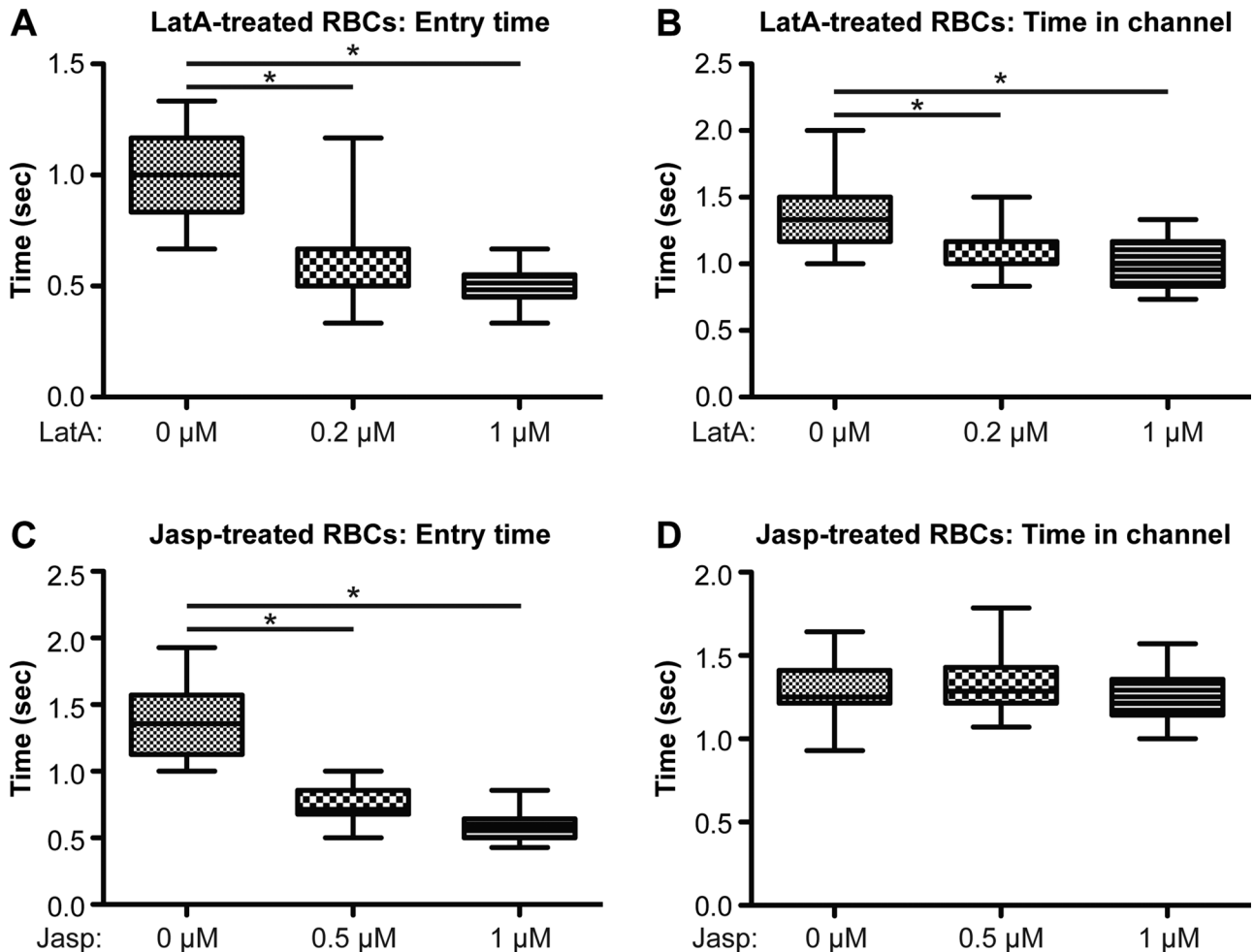
FIGURE 6: LatA and Jasp treatment have differential effects on entry time vs. persistence time in a microfluidic channel. Boxplots depict (A, C) RBC entry times and (B, D) persistence times in a microfluidic channel for RBCs treated with the indicated concentrations of (A, B) LatA or (C, D) Jasp. Note that LatA treatment decreases both entry time and persistence time in the channel, whereas Jasp treatment only decreases entry time, with no effect on persistence time in the channel. Each boxplot reflects $n \geq 30$ RBCs. *$p < 0.01$. Note that RBCs in A and B vs. C and D were obtained from different human donors and hence have slightly different entry time and persistence time in the presence of DMSO alone.

RBC transit time in a microfluidic channel can be expressed as the entry time (i.e., time required for initial RBC shape change upon channel entry) plus the persistence time in the channel before egress from the channel. When we compared these distinct modes of RBC kinematics, we observed that LatA treatment decreases both entry time and persistence time in the channel, whereas Jasp treatment only decreases entry time, with little effect on persistence time in the channel (Figure 6). We conclude that reduced transit time of LatA-treated RBCs is attributable to both reduced entry time and persistence time in the channel, whereas reduced transit time of Jasp-treated RBCs is solely attributable to reduced entry time.

Next we used LatA and Jasp treatment to examine the role of actin filament assembly and disassembly in RBC flickering—spontaneous oscillations of the RBC membrane (Levin and Korenstein, 1991; Tuvia et al., 1998; Costa et al., 2008; Betz et al., 2009)—which are reduced via CytoD inhibition of F-actin's ATPase activity (Tuvia et al., 1998). We analyzed RBC flickering by phase-contrast video microscopy of biconcave RBCs, with computational analysis of the coefficient of variance over time for the amplitudes of RBC membrane oscillations (Figure 7A; Ghiran et al., 2011). We found that F-actin disassembly induced via treatment with 1 µM LatA significantly

increased the variance of flickering, whereas F-actin stabilization via treatment with 1 µM Jasp had the opposite effect (Figure 7, B and C). Therefore actin filament stability is inversely related to the variance of flickering. This result differs from our microfluidic channel assays, for which F-actin destabilization via LatA treatment and F-actin stabilization via Jasp treatment induced nearly identical increases in RBC deformability (Figure 5). Collectively our microfluidic channel and flickering assays support a model in which different actin filament subpopulations are differentially assembled and disassembled in different modes of RBC kinematics.

DISCUSSION

Filament-level actin subunit dynamics in RBCs

Research on RBCs has long assumed that membrane skeleton-associated actin filaments are static and do not undergo dynamic subunit exchange (Fowler, 2013). However, our data challenge this dogma and argue in favor of dynamic actin subunit exchange between the cytosol and an actin filament subpopulation in the RBC membrane skeleton, mediated by barbed-end dynamics. First, the soluble actin concentration in RBCs (0.36 µM) is between the barbed-end and pointed-end critical concentrations of 0.1 and
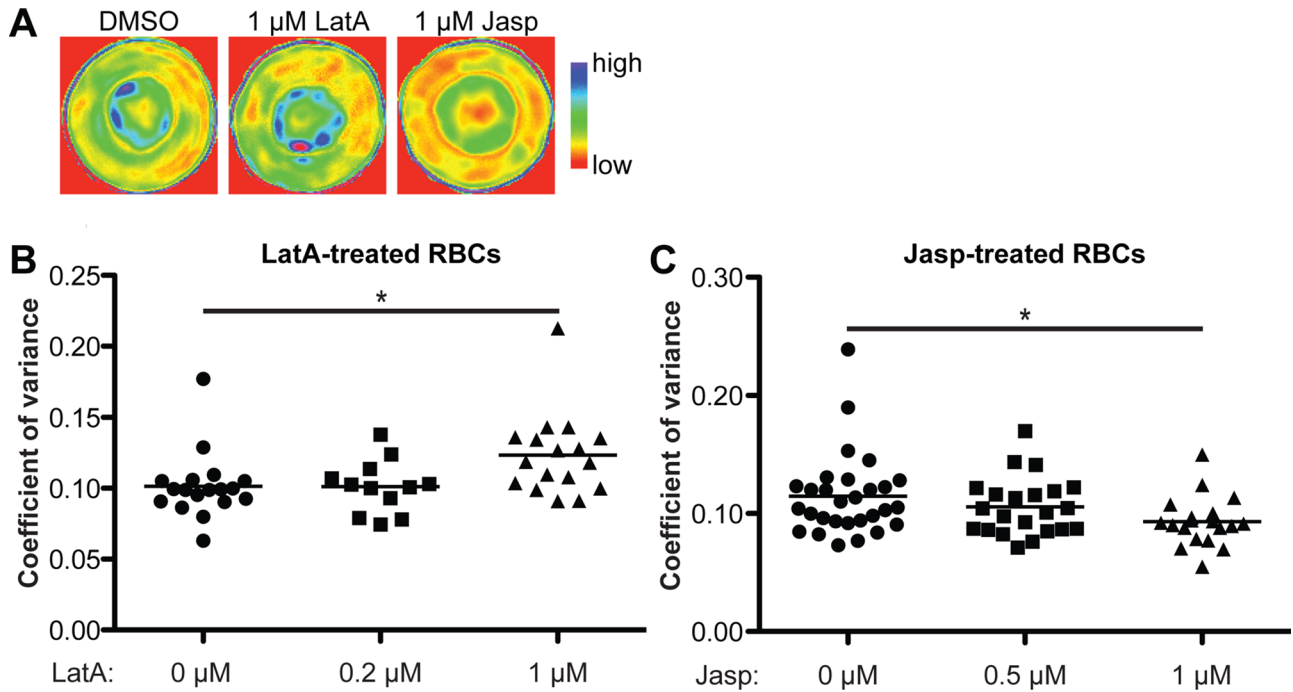
FIGURE 7: LatA and Jasp treatment have differential effects on the membrane flickering of human RBCs. (A) Example heat maps depicting variances of flickering amplitudes across the RBC surface. (B, C) Dotplots depict coefficients of variance of flickering amplitudes for RBCs treated with the indicated concentrations of (B) LatA or (C) Jasp. Note that LatA treatment increases the variance of flickering amplitudes, whereas Jasp treatment decreases the variance of flickering amplitudes. Each dot represents data from one RBC. *$p < 0.05$. Note that RBCs in B and C were obtained from different human donors and hence have slightly different variances of flickering amplitudes in the presence of DMSO alone.

0.6 µM, respectively (Pollard *et al.*, 2000). Second, we observed that CytoD treatment inhibits rho-actin incorporation at discrete foci in the membrane skeleton of RBC ghosts. These experiments were performed with RBCs from adult peripheral blood, with minimal (<1%) contamination by reticulocytes, which lack a mature spectrin-actin membrane skeleton with its full cohort of associated actin-binding proteins (Chasis *et al.*, 1989; Kaushansky *et al.*, 2010; Liu *et al.*, 2010). Thus barbed-end exchange appears to be the predominant mechanism facilitating dynamic actin subunit incorporation into the RBC membrane skeleton. Moreover, an RBC cytosolic actin concentration intermediate with respect to the barbed-end and pointed-end critical concentrations suggests that at least some RBC actin filaments might undergo treadmilling (i.e., subunit assembly at barbed ends with disassembly at pointed ends; Bugyi and Carlier, 2010).

Although our data do not allow us to determine whether many filaments partially assemble or disassemble or whether small numbers of entire filaments polymerize or depolymerize, it is instructive to compare the changes in cytosolic actin with the amount of polymerized actin filaments in the membrane skeleton. For example, our drug treatment experiments indicate that the fraction of actin subunits capable of assembling and disassembling from RBC actin filaments via barbed-end exchange is rather low. The approximately twofold increase in soluble actin after LatA treatment reflects an increase from 3.7% to 7.4% soluble actin over the 4-h incubation at 37°C used here, corresponding to depolymerization of ~1000–1600 whole filaments out of a population of ~30,000–40,000 filaments in the membrane skeleton, or, alternatively, slightly <1 subunit from each of the 30,000–40,000 filaments (Fowler, 1996). Similarly, the ~60% decrease in soluble actin after Jasp treatment reflects a decrease from 3.7% to 1.5% soluble actin, corresponding to polymer-

ization of ~600–900 new filaments in the membrane skeleton, or <1 subunit onto each of the 30,000–40,000 filaments (Fowler, 1996). Such subtle changes in F-actin content and organization in response to actin-disrupting drugs differ markedly from the robust changes in F-actin organization observed in LatA- and Jasp-treated nonerythroid cells (Ayscough *et al.*, 1997; Bubb *et al.*, 2000; Pappas *et al.*, 2010) and may reflect specialization of the spectrin-based membrane skeleton. Our calculations, in conjunction with the observed foci of rho-actin incorporation into RBC ghosts, favor the existence of dynamic subpopulations or "hotspots" within the membrane skeleton where actin filaments assemble and disassemble, rather than uniform turnover across the entire RBC actin network.

Network-level actin filament mobility in RBCs

Our FRAP experiments also revealed a previously unrecognized long-range mobility of the RBC actin filament network. The simplest explanation for F-actin mobility in the spectrin-actin membrane skeleton of a quiescent biconcave RBC might be the occurrence of stochastic spreading and unspreading events within the network, facilitated by conformational changes in the $(\alpha_1\beta_1)_2$-spectrin strands (Bloch and Pumplin, 1992). During such events, rearrangements of $(\alpha_1\beta_1)_2$-spectrin strands would presumably be driven by lateral movements of ankyrin/band3 complexes in the lipid bilayer (Golan and Veatch, 1980; Kodippili *et al.*, 2009, 2012). This, in turn, would result in lateral displacement of $(\alpha_1\beta_1)_2$-spectrin-bound actin filaments. Occurrence of such events would also imply that the degree of spreading of the RBC membrane skeleton is heterogeneous across the RBC membrane, which could lead to spatial heterogeneities in the force distribution across the membrane, possibly driving RBC membrane curvature and biconcave shape (Mohandas *et al.*, 1983; Mohandas and Chasis, 1993).

An alternative explanation for the observed F-actin mobility in RBCs would be spontaneous dissociation/reassociation of $(\alpha_1\beta_1)_2$-spectrin/F-actin linkages, leading to changes in membrane skeleton architecture and actin filament positioning. However, the presence of five to seven high-affinity $(\alpha_1\beta_1)_2$-spectrin attachments on each RBC actin filament appears to make such events relatively unlikely (Bennett and Baines, 2001; Fowler, 2013). It also remains unclear why inhibition of barbed-end actin exchange at the single-filament level via CytoD treatment results in a small but statistically significant decrease in the mobile fraction of F-actin at the membrane-skeleton level. A possibility is that barbed-end assembly (i.e., more ATP-actin subunits) might influence the affinity of $(\alpha_1\beta_1)_2$-spectrin for F-actin or that CytoD preferentially binds to and directly alters the mobility of a biochemically distinct subset of mobile RBC actin filaments. Additional biochemical experiments are required to distinguish among these or other possibilities.

It is instructive to compare actin mobility in RBCs with actin mobility in nonerythroid cells. RBC actin filaments are structurally similar to the thin filaments of striated muscle sarcomeres in that they are both long-lived cytoskeletal structures, have precisely regulated and highly uniform lengths, are capped at both ends, and are coated along their length with tropomyosin (Fowler, 1996). However, sarcomeric thin filaments are many times longer than RBC actin filaments (~1 μm vs. 37 nm long, respectively) and exhibit both barbed-end and pointed-end assembly when rho-actin is microinjected into living myocytes (Littlefield et al., 2001), unlike RBC actin filaments, which only exhibit barbed-end assembly when RBC ghosts are resealed in the presence of rho-actin. Nevertheless, FRAP analysis of sarcomeric thin filaments in cultured cardiomyocytes and skeletal myvotubes expressing GFP-actin has identified a mobile actin fraction of ~25% and fluorescence recovery occurring on the minutes time scale (Littlefield et al., 2001; Skwarek-Maruszewska et al., 2009; Pappas et al., 2010), similar to our findings in RBCs. By contrast, FRAP analysis of the highly dynamic, dendritic actin filament network in the lamellipodium of migrating cells identifies an actin mobile fraction of nearly 100% and fluorescence recovery occurring within seconds (Lai et al., 2008). Collectively these studies argue against simple categorization of actin filament structures as either "static" or "dynamic" and instead favor a continuum of dynamic states on which both short- and long-lived actin filament structures might reside.

Actin filament function in RBC biomechanics

We confirmed that it is possible to perturb F-actin assembly/disassembly in RBCs via treatment with LatA or Jasp, consistent with these drugs' destabilizing or stabilizing effects on dynamic actin filaments, respectively (Coue et al., 1987; Spector et al., 1989; Bubb et al., 1994, 2000; Morton et al., 2000; Holzinger, 2009). We exploited this in our biomechanical assays, which revealed that RBC actin filaments play important roles in specific modes of RBC deformation. Neither LatA nor Jasp treatment affected RBC osmotic fragility, indicating unchanged membrane extensibility and ratio of surface area to volume (Kaushansky et al., 2010), but both LatA and Jasp treatment increased membrane deformability, as determined by a microfluidic channel assay. Moreover, our data are the first to reveal different modes of RBC actin filament function during passage through a microfluidic channel—namely, microchannel entry time is both LatA and Jasp sensitive, whereas persistence time in the microchannel is LatA but not Jasp sensitive, suggesting that different subpopulations of actin filaments with different assembly/disassembly and mechanical properties are recruited during each of these functional modes.

The importance of RBC actin filaments in regulating RBC deformability was first suggested by experiments showing abnormal membrane deformability in resealed RBC ghosts treated with phalloidin (Nakashima and Beutler, 1979), which has a similar actin filament–stabilizing effect as Jasp, and later by a series of gene-targeted mouse models lacking various actin-capping proteins in RBCs (Gilligan et al., 1999; Muro et al., 2000; Porro et al., 2004; Chen et al., 2007; Robledo et al., 2008; Moyer et al., 2010). (Treatment with a CytoD analogue, CytoB, has also been shown to increase RBC osmotic fragility and membrane deformability [Beck et al., 1972], but this could be due to off-target binding to the glucose transporter and metabolic effects [Bloch, 1973; Taverna and Langdon, 1973; Lin and Spudich, 1974; Jung and Rampal, 1977].) Increased RBC deformability due to LatA or Jasp treatment could be due to changes in the number and/or steric accessibility of $(\alpha_1\beta_1)_2$-spectrin-binding sites on some of the short actin filaments, which may lead to rearrangement of the spectrin-actin lattice and suboptimal force distribution across the plasma membrane. Such a mechanism is consistent with mathematical modeling of RBC actin filament nodes, whose mechanical behavior is sensitive to the spatial arrangement of $(\alpha_1\beta_1)_2$-spectrin attachments (Sung and Vera, 2003; Vera et al., 2005).

In addition to increasing deformability, we also discovered that LatA or Jasp treatment increases or decreases the variance of intact RBC membrane flickering amplitudes, respectively (i.e., actin filament stability is inversely related to the variance of flickering). This extends work by Tuvia et al. (1998) showing that phalloidin treatment, which is expected to have a similar effect as Jasp treatment, decreases the variance of flickering in RBC ghosts. However, results by Betz et al. (2009) differed from ours in that they showed that no effect of LatA on flickering; we attribute this difference to the fact that they examined solely flickering amplitudes, whereas we focused on flickering variances. We propose two possible models: 1) Actin filament assembly/disassembly in the proximity of the RBC membrane may result in transient contacts between the lipid bilayer and dynamic actin subunits at filament ends, which, when integrated over space and time, manifest as 0.2- to 30-Hz flickering events (Brochard and Lennon, 1975). 2) Alternatively, actin filament assembly "pushing" on the lipid bilayer may stabilize the bilayer by enhancing membrane tension. Such a pushing mechanism might contribute to the spatial heterogeneity of the biomechanical properties of the membrane (Picas et al., 2013). Future work will require careful biophysical approaches and analyses of RBCs with targeted deletions of actin-binding proteins to understand the structural basis for actin filament recruitment and force transmission that underlie RBC biomechanical properties and shapes.

MATERIALS AND METHODS
RBC handling
Human blood was drawn into BD Vacutainer tubes spray coated with K_2EDTA at the Normal Blood Donor Service at the Scripps Research Institute (La Jolla, CA), according to an Institutional Review Board–approved protocol for blood collection from human subjects (11-5773). Freshly drawn blood was centrifuged for 10 min at $1000 \times g$, serum and buffy coat were aspirated off, and RBCs were resuspended in 20 volumes of 4-(2-hydroxyethyl)-1-piperazineethanesulfonic acid (HEPES)–buffered saline (HBS) optimized for human RBCs (145 mM NaCl, 5 mM KCl, 1 mM $MgCl_2$, 10 mM glucose, 10 mM HEPES, 2 mM adenosine, pH 7.4). RBCs were washed three times by centrifugation at $1000 \times g$, aspiration of the supernatant, and resuspension in 20 volumes of HBS. Washed RBCs were then stored on ice for up to 2 d. In some experiments,

membrane skeletons were prepared from washed RBCs or ghosts by addition of four volumes of Triton-lysis buffer (145 mM NaCl, 5 nM KCl, 1 mM MgCl$_2$, 10 mM HEPES, 5 mM dithiothreitol [DTT], 2.5% Triton X-100, pH 7.4) and protease inhibitor cocktail (1:1000; Sigma-Aldrich, St. Louis, MO) to the packed cells, followed by centrifugation of the membrane skeletons at 15,000 × g through an underlaid shelf of Triton-lysis buffer plus 20% sucrose and subsequent separation of supernatants and pellets.

Actin-disrupting drugs

CytoD, LatA, and Jasp were purchased from Sigma-Aldrich, and stock solutions were prepared in DMSO and stored at –20°C until use.

Rho-actin incorporation

Rho-actin was prepared from purified rabbit skeletal muscle actin by labeling on cysteine 374 as described (Tait and Frieden, 1982; Littlefield et al., 2001). Rho-actin was labeled at an efficiency of ~0.3 mol rhodamine/mol actin and stored in liquid N$_2$ at 5 mg/ml in a buffer containing 4 mM Tris, 0.1 mM CaCl$_2$, 0.2 mM Mg$_2$ATP, 2 mM DTT, and 0.02% NaN$_3$ (pH 8.0). RBCs were washed three times in phosphate-buffered saline (PBS) at 4°C, resuspended to 10% hematocrit in PBS, and pretreated with 0.5 µM CytoD in 0.001% DMSO, DMSO alone, or no additions for 30 min at room temperature in PBS. RBCs were collected by sedimentation in an Eppendorf microfuge, the supernatant was removed, and RBCs were lysed by adding 10 µl of packed RBCs to 40 µl of 0.5 mM Mg$_2$ATP and 10 mM sodium phosphate (pH 7.4) containing 2.4 µM rho-actin with or without 0.5 µM CytoD (final concentration) and incubated for 10 min on ice. Lysed RBCs were resealed by the addition of 5 µl of 1 M KCl and 10 mM MgCl$_2$ for 30 min at 37°C, followed by the addition of 1 ml of cold PBS and centrifugation for 5 min at 12,000 rpm in an Eppendorf microfuge to remove excess extracellular rho-actin. Note that this and all subsequent wash buffers contained 500 nM CytoD or DMSO, as appropriate. Resealed ghosts were washed twice in PBS with 0.01% bovine serum albumin (PBS/BSA) at 4°C by resuspension and sedimentation and then resuspended in 800 µl PBS/BSA.

In some experiments, 200 µl of the ghost suspension was allowed to settle onto a carbonate-coated coverslip for 30 min at room temperature. Ultraclean "squeaky clean" coverslips were prepared as described (Waterman-Storer, 2001) and carbonate coated as described (Perlmann et al., 1984). Excess fluid was aspirated off, and coverslips were washed in 200 µl of PBS/BSA, fixed in 1.6% paraformaldehyde (PFA) in PBS for 15 min at room temperature, and then washed twice in PBS. Ghosts were observed as wet mounts with a Zeiss Axioskop fluorescence microscope using a 63× Plan-Apochromat oil-immersion objective lens (numerical aperture [NA] 1.4) with an Optovar setting of 1.6. Images were collected with a 20-s exposure time using a charge-coupled device (CCD) camera and a Y1300 Interline chip (Princeton Instruments, Trenton, NJ). In other experiments, 10 µl of the ghost suspension was used to prepare membrane skeletons, as described, and subjected to Western blotting, as follows.

Western blotting

Washed RBCs in HBS were incubated for 4 h in a 37°C water bath in the presence of DMSO or the indicated drugs. The supernatants (soluble fractions) of Triton-lysis buffer–extracted RBCs were separated from the pellets (membrane skeleton fractions) as described. Soluble fractions were solubilized in 1/5 volume of 5× SDS sample buffer, boiled for 5 min, electrophoretically separated on 4–20% Tris-glycine gradient minigels for 1 h at 200 V, and transferred to nitrocellulose (pore size, 0.2 µm) in transfer buffer contain-

ing 20% methanol. Blots were stained with 0.2% Ponceau S in 3% trichloroacetic acid to control for loading, blocked for 2 h in 4% BSA plus 1% goat serum in PBS at room temperature, and then incubated in primary antibody diluted in Blitz buffer (4% BSA, 10 mM NaHPO$_4$, 150 mM NaCl, 1 mM EDTA, 0.2% Triton X-100, pH 7.4) overnight at 4°C. Primary antibodies were as follows: mouse monoclonal anti-actin (C4, 1:10,000; EMD Millipore, Billerica, MA), mouse monoclonal anti-rhodamine (11H10, 1:1000; Santa Cruz Biotechnology, Dallas, TX), mouse monoclonal anti–β-actin (AC-74, 1:1000; Sigma-Aldrich), rabbit polyclonal anti-human Tmod1 (R1749bl3c, 1:1000; Moyer et al., 2010), rabbit polyclonal anti–α-adducin (1:1000; a gift from Vann Bennett, Duke University, Durham, NC), and sheep polyclonal anti-TM5NM1 (AB5447, 1:1000; EMD Millipore). After washing in PBS plus 0.1% Triton X-100, blots were incubated in either horseradish peroxidase– or 680LT-conjugated secondary antibody diluted in Blitz for 1 h at room temperature. After washing again in PBS plus 0.1% Triton X-100, bands were visualized either using enhanced chemiluminescence followed by exposure to film or a LI-COR Odyssey infrared imaging system. Background-corrected band intensities were densitometrically quantified using ImageJ. Western band intensities were normalized to the sum of the intensities of the nonhemoglobin bands on the corresponding Ponceau S–stained blot.

TIRF microscopy

RBCs washed in HBS with glucose and adenosine (see earlier description) were incubated for 4 h in a 37°C water bath in the presence of DMSO or the indicated drugs. RBCs were then fixed overnight in 4% PFA at 4°C, washed three times in HBS, permeabilized for 10 min in 0.3% Triton X-100, blocked in 4% BSA plus 1% goat serum, and stained with Alexa 488–phalloidin (Life Technologies, Carlsbad, CA) for F-actin. After additional washing, RBCs were deposited onto glass slides using a Thermo-Fisher Cytospin 4 Cytocentrifuge at 1000 rpm for 3 min, and coverslips were mounted onto the slides using Fluoro-Gel aqueous mounting medium (Electron Microscopy Sciences, Hatfield, PA). Images were collected at room temperature on a Nikon Eclipse Ti inverted microscope with a 100× Apochromat oil objective lens (NA 1.49) and TIRF illumination in conjunction with a Photometrics CoolSNAP HQ2 CCD camera (Roper Scientific, Tucson, AZ). Images were collected using NIS-Elements 3.2 software (Nikon, Melville, NY) and processed using Volocity 5.3.2 software (Improvision, Waltham, MA).

FRAP

RBC actin filaments were labeled by incubating washed RBCs (1 × 10^9 RBCs at a hematocrit of 10%) in Ca^{2+}- and Mg^{2+}-containing Hank's balanced salt solution (HBSS) supplemented with 1 µM SiR-Jasp (Lukinavicius et al., 2014) for 30 min at room temperature. In some experiments, RBCs were fixed in 0.5% acrolein for 5 min at room temperature before SiR-Jasp staining (Melhorn et al., 2013). Cells were then washed twice, resuspended in HBSS containing 0.05% immunoglobulin G–free BSA, and seeded on a slide for 5 min before FRAP analysis. Images were acquired at a rate of 1 image/min using a 60× UPlanApo objective (NA 1.42) mounted on an Olympus BX62 microscope and a cooled QImaging Emc^2 electron-multiplying CCD camera. FRAP was performed using a 488-nm Laser Vector Photomanipulation unit controlled by SlideBook 5.5 software (Intelligent Imaging Innovations, Denver, CO) and analyzed using Slidebook's FRAP analysis module, as described previously (Melhorn et al., 2013). At least 20 RBCs were analyzed for each condition. RBCs that did not have a standard biconcave shape were excluded from analysis.

Osmotic fragility

Lysis of intact RBCs as a function of osmolarity was measured as previously described (Gilligan *et al.*, 1999; Moyer *et al.*, 2010). Briefly, washed RBCs were treated with DMSO or the indicated drugs and then diluted to a final hematocrit of 5% in HBS. Small volumes of the RBC suspension (10 μl) were diluted in buffers of known osmolarities (range 0–280 mOsm/l, pH 7.4), incubated at room temperature for 20 min, and centrifuged for 5 min at $1000 \times g$. Supernatants were removed and transferred to 96-well plates, and percentage lysis was calculated from the absorbance at 540 nm.

Microfluidic measurement of RBC deformability

Two-dimensional microfluidic arrays were used as previously described (Ghiran *et al.*, 2011). Briefly, washed RBCs (5 μl) were loaded into the inlet reservoir of a microchannel and driven into a capillary-like area by lowering the reservoir tube on the opposite side of the apparatus. Once RBCs reached the microchannel, the reservoir was raised to an appropriate height that allowed control RBCs from healthy donors to pass through the length (25 μm) of the capillary in ~3 s. The cells were video recorded using a 40× Ph2 Plan Fluorite objective (NA 0.75) mounted on a TE300 Nikon inverted microscope, using a QImaging Retiga EXi CCD camera controlled by iVision 4.7 software (BioVision Technologies, Exton, PA) at a rate of 10 frames/s. Movies were analyzed offline, frame by frame, and any RBCs that were unusually shaped, overlapped, or clustered were excluded from measurement. At least 30 RBCs were counted for each experimental condition.

Membrane flickering analysis

Spontaneous RBC membrane oscillations (flickering) were measured as previously described (Ghiran *et al.*, 2011). Positive-low, phase-contrast, time-lapse images of RBCs seeded on microscope slides were recorded for 10 s at a rate of 33 frames/s using a 100× UPlanApo phase contrast objective (NA 1.35) on an Olympus BX62 microscope. Flickering was measured using iVision 4.0.9 software (BioVision Technologies). At the end of each recording, an intensity projection step of the image stack was performed to identify and exclude RBCs that drifted during recording. The intensity of scattered light was used to calculate, pixel by pixel, the coefficient of variance at each point within the RBC and display the results as a pseudocolor amplitude map.

Statistics

Significant differences between two groups were detected using Student's *t* test. Significant differences among three or more groups were detected using one-way analysis of variance with post hoc Fisher's protected least significant difference tests. Statistical analysis was performed in Excel (Microsoft, Redmond, WA). Significance was defined as $p < 0.05$.

REFERENCES

Allingham JS, Klenchin VA, Rayment I (2006). Actin-targeting natural products: structures, properties and mechanisms of action. Cell Mol Life Sci 63, 2119–2134.

Ayscough KR, Stryker J, Pokala N, Sanders M, Crews P, Drubin DG (1997). High rates of actin filament turnover in budding yeast and roles for actin in establishment and maintenance of cell polarity revealed using the actin inhibitor latrunculin-A. J Cell Biol 137, 399–416.

Beck JS, Jay AW, Saari JT (1972). Effects of cytochalasin B on osmotic fragility and deformability of human erythrocytes. Can J Physiol Pharmacol 50, 684–688.

Bennett V, Baines AJ (2001). Spectrin and ankyrin-based pathways: metazoan inventions for integrating cells into tissues. Physiol Rev 81, 1353–1392.

Bennett V, Gilligan DM (1993). The spectrin-based membrane skeleton and micron-scale organization of the plasma membrane. Annu Rev Cell Biol 9, 27–66.

Bennett V, Lorenzo DN (2013). Spectrin- and ankyrin-based membrane domains and the evolution of vertebrates. Curr Top Membr 72, 1–37.

Betz T, Lenz M, Joanny JF, Sykes C (2009). ATP-dependent mechanics of red blood cells. Proc Natl Acad Sci USA 106, 15320–15325.

Bloch R (1973). Inhibition of glucose transport in the human erythrocyte by cytochalasin B. Biochemistry 12, 4799–4801.

Bloch RJ, Pumplin DW (1992). A model of spectrin as a concertina in the erythrocyte membrane skeleton. Trends Cell Biol 2, 186–189.

Brochard F, Lennon JF (1975). Frequency spectrum of the flicker phenomenon in erythrocytes. J Phys (France) 36, 1035–1047.

Bubb MR, Senderowicz AM, Sausville EA, Duncan KL, Korn ED (1994). Jasplakinolide, a cytotoxic natural product, induces actin polymerization and competitively inhibits the binding of phalloidin to F-actin. J Biol Chem 269, 14869–14871.

Bubb MR, Spector I, Beyer BB, Fosen KM (2000). Effects of jasplakinolide on the kinetics of actin polymerization. An explanation for certain in vivo observations. J Biol Chem 275, 5163–5170.

Bugyi B, Carlier MF (2010). Control of actin filament treadmilling in cell motility. Annu Rev Biophys 39, 449–470.

Burton AL, Anderson WL, Andrews RV (1968). Quantitative studies on the flicker phenomenon in the erythrocytes. Blood 32, 819–822.

Chasis JA, Prenant M, Leung A, Mohandas N (1989). Membrane assembly and remodeling during reticulocyte maturation. Blood 74, 1112–1120.

Chen H, Khan AA, Liu F, Gilligan DM, Peters LL, Messick J, Haschek-Hock WM, Li X, Ostafin AE, Chishti AH (2007). Combined deletion of mouse dematin-headpiece and beta-adducin exerts a novel effect on the spectrin-actin junctions leading to erythrocyte fragility and hemolytic anemia. J Biol Chem 282, 4124–4135.

Cooper JA (1987). Effects of cytochalasin and phalloidin on actin. J Cell Biol 105, 1473–1478.

Costa M, Ghiran I, Peng CK, Nicholson-Weller A, Goldberger AL (2008). Complex dynamics of human red blood cell flickering: alterations with in vivo aging. Phys Rev E Stat Nonlin Soft Matter Phys 78, 020901.

Coue M, Brenner SL, Spector I, Korn ED (1987). Inhibition of actin polymerization by latrunculin A. FEBS Lett 213, 316–318.

Cyrklaff M, Sanchez CP, Kilian N, Bisseye C, Simpore J, Frischknecht F, Lanzer M (2011). Hemoglobins S and C interfere with actin remodeling in Plasmodium falciparum-infected erythrocytes. Science 334, 1283–1286.

Fischer RS, Fritz-Six KL, Fowler VM (2003). Pointed-end capping by tropomodulin3 negatively regulates endothelial cell motility. J Cell Biol 161, 371–380.

Fowler VM (1996). Regulation of actin filament length in erythrocytes and striated muscle. Curr Open Cell Biol 8, 86–96.

Fowler VM (2013). The human erythrocyte plasma membrane: a Rosetta Stone for decoding membrane-cytoskeleton structure. Curr Top Membr 72, 39–88.

Ghiran IC, Zeidel ML, Shevkoplyas SS, Burns JM, Tsokos GC, Kyttaris VC (2011). Systemic lupus erythematosus serum deposits C4d on red blood cells, decreases red blood cell membrane deformability, promotes nitric oxide production. Arthritis Rheum 63, 503–512.

Gilligan DM, Lozovatsky L, Gwynn B, Brugnara C, Mohandas N, Peters LL (1999). Targeted disruption of the beta adducin gene (Add2) causes red blood cell spherocytosis in mice. Proc Natl Acad Sci USA 96, 10717–10722.

Gokhin DS, Fowler VM (2011). Cytoplasmic gamma-actin and tropomodulin isoforms link to the sarcoplasmic reticulum in skeletal muscle fibers. J Cell Biol 194, 105–120.

Golan DE, Veatch W (1980). Lateral mobility of band 3 in the human erythrocyte membrane studied by fluorescence photobleaching recovery:

evidence for control by cytoskeletal interactions. Proc Natl Acad Sci USA 77, 2537–2541.

Hinshaw DB, Burger JM, Miller MT, Adams JA, Beals TF, Omann GM (1993). ATP depletion induces an increase in the assembly of a labile pool of polymerized actin in endothelial cells. Am J Physiol 264, C1171–C1179.

Holzinger A (2009). Jasplakinolide: an actin-specific reagent that promotes actin polymerization. Methods Mol Biol 586, 71–87.

Jung CY, Rampal AL (1977). Cytochalasin B binding sites and glucose transport carrier in human erythrocyte ghosts. J Biol Chem 252, 5456–5463.

Kaushansky K, Lichtman MA, Beutler E, Kipps TJ, Seligsohn U, Prchal JT (2010). Williams Hematology, McGraw-Hill Medical: New York.

Kodippili GC, Spector J, Hale J, Giger K, Hughes MR, McNagny KM, Birkenmeier C, Peters L, Ritchie K, Low PS (2012). Analysis of the mobilities of band 3 populations associated with ankyrin protein and junctional complexes in intact murine erythrocytes. J Biol Chem 287, 4129–4138.

Kodippili GC, Spector J, Sullivan C, Kuypers FA, Labotka R, Gallagher PG, Ritchie K, Low PS (2009). Imaging of the diffusion of single band 3 molecules on normal and mutant erythrocytes. Blood 113, 6237–6245.

Lai FP, Szczodrak M, Block J, Faix J, Breitsprecher D, Mannherz HG, Stradal TE, Dunn GA, Small JV, Rottner K (2008). Arp2/3 complex interactions and actin network turnover in lamellipodia. EMBO J 27, 982–992.

Levin S, Korenstein R (1991). Membrane fluctuations in erythrocytes are linked to MgATP-dependent dynamic assembly of the membrane skeleton. Biophys J 60, 733–737.

Lin S, Spudich JA (1974). Biochemical studies on the mode of action of cytochalasin B. Cytochalasin B binding to red cell membrane in relation to glucose transport. J Biol Chem 249, 5778–5783.

Littlefield R, Almenar-Queralt A, Fowler VM (2001). Actin dynamics at pointed ends regulates thin filament length in striated muscle. Nat Cell Biol 3, 544–551.

Liu J, Guo X, Mohandas N, Chasis JA, An X (2010). Membrane remodeling during reticulocyte maturation. Blood 115, 2021–2027.

Liu F, Khan AA, Chishti AH, Ostafin AE (2011). Atomic force microscopy demonstration of cytoskeleton instability in mouse erythrocytes with dematin-headpiece and beta-adducin deficiency. Scanning 33, 426–436.

Lukinavicius G, Reymond L, D'Este E, Masharina A, Gottfert F, Ta H, Guther A, Fournier M, Rizzo S, Waldmann H, et al. (2014). Fluorogenic probes for live-cell imaging of the cytoskeleton. Nat Methods 11, 731–733.

MacLean-Fletcher S, Pollard TD (1980). Mechanism of action of cytochalasin B on actin. Cell 20, 329–341.

Melhorn MI, Brodsky AS, Estanislau J, Khoory JA, Illigens B, Hamachi I, Kurishita Y, Fraser AD, Nicholson-Weller A, Dolmatova E, et al. (2013). CR1-mediated ATP release by human red blood cells promotes CR1 clustering and modulates the immune transfer process. J Biol Chem 288, 31139–31153.

Mohandas N, Chasis JA (1993). Red blood cell deformability, membrane material properties and shape: regulation by transmembrane, skeletal and cytosolic proteins and lipids. Semin Hematol 30, 171–192.

Mohandas N, Chasis JA, Shohet SB (1983). The influence of membrane skeleton on red cell deformability, membrane material properties, and shape. Semin Hematol 20, 225–242.

Morton WM, Ayscough KR, McLaughlin PJ (2000). Latrunculin alters the actin-monomer subunit interface to prevent polymerization. Nat Cell Biol 2, 376–378.

Moyer JD, Nowak RB, Kim NE, Larkin SK, Peters LL, Hartwig J, Kuypers FA, Fowler VM (2010). Tropomodulin 1-null mice have a mild spherocytic elliptocytosis with appearance of tropomodulin 3 in red blood cells and disruption of the membrane skeleton. Blood 116, 2590–2599.

Muro AF, Marro ML, Gajovic S, Porro F, Luzzatto L, Baralle FE (2000). Mild spherocytic hereditary elliptocytosis and altered levels of alpha- and gamma-adducins in beta-adducin-deficient mice. Blood 95, 3978–3985.

Nakashima K, Beutler E (1979). Comparison of structure and function of human erythrocyte and human muscle actin. Proc Natl Acad Sci USA 76, 935–938.

Pappas CT, Krieg PA, Gregorio CC (2010). Nebulin regulates actin filament lengths by a stabilization mechanism. J Cell Biol 189, 859–870.

Perlmann H, Berzins K, Wahlgren M, Carlsson J, Bjorkman A, Patarroyo ME, Perlmann P (1984). Antibodies in malarial sera to parasite antigens in the membrane of erythrocytes infected with early asexual stages of Plasmodium falciparum. J Exp Med 159, 1686–1704.

Picas L, Rico F, Deforet M, Scheuring S (2013). Structural and mechanical heterogeneity of the erythrocyte membrane reveals hallmarks of membrane stability. ACS Nano 7, 1054–1063.

Pinder JC, Clark SE, Baines AJ, Morris E, Gratzer WB (1981). The construction of the red cell cytoskeleton. Prog Clin Biol Res 55, 343–361.

Pinder JC, Gratzer WB (1983). Structural and dynamic states of actin in the erythrocyte. J Cell Biol 96, 768–775.

Pollard TD, Blanchoin L, Mullins RD (2000). Molecular mechanisms controlling actin filament dynamics in nonmuscle cells. Annu Rev Biophys Biomol Struct 29, 545–576.

Porro F, Costessi L, Marro ML, Baralle FE, Muro AF (2004). The erythrocyte skeletons of beta-adducin deficient mice have altered levels of tropomyosin, tropomodulin and EcapZ. FEBS Lett 576, 36–40.

Quadri SK, Sun L, Islam MN, Shapiro L, Bhattacharya J (2012). Cadherin selectivity filter regulates endothelial sieving properties. Nat Commun 3, 1099.

Reits EA, Neefjes JJ (2001). From fixed to FRAP: measuring protein mobility and activity in living cells. Nat Cell Biol 3, E145–147.

Robledo RF, Ciciotte SL, Gwynn B, Sahr KE, Gilligan DM, Mohandas N, Peters LL (2008). Targeted deletion of alpha-adducin results in absent beta- and gamma-adducin, compensated hemolytic anemia, and lethal hydrocephalus in mice. Blood 112, 4298–4307.

Rug M, Cyrklaff M, Mikkonen A, Lemgruber L, Kuelzer S, Sanchez CP, Thompson J, Hanssen E, O'Neill M, Langer C, et al. (2014). Export of virulence proteins by malaria-infected erythrocytes involves remodeling of host actin cytoskeleton. Blood 124, 3459–3468.

Sampath P, Pollard TD (1991). Effects of cytochalasin, phalloidin, and pH on the elongation of actin filaments. Biochemistry 30, 1973–1980.

Shevkoplyas SS, Gifford SC, Yoshida T, Bitensky MW (2003). Prototype of an in vitro model of the microcirculation. Microvasc Res 65, 132–136.

Shevkoplyas SS, Yoshida T, Gifford SC, Bitensky MW (2006). Direct measurement of the impact of impaired erythrocyte deformability on microvascular network perfusion in a microfluidic device. Lab Chip 6, 914–920.

Skwarek-Maruszewska A, Hotulainen P, Mattila PK, Lappalainen P (2009). Contractility-dependent actin dynamics in cardiomyocyte sarcomeres. J Cell Sci 122, 2119–2126.

Spector I, Shochet NR, Blasberger D, Kashman Y (1989). Latrunculins—novel marine macrolides that disrupt microfilament organization and affect cell growth: I. Comparison with cytochalasin D. Cell Motil Cytoskeleton 13, 127–144.

Sung LA, Vera C (2003). Protofilament and hexagon: a three-dimensional mechanical model for the junctional complex in the erythrocyte membrane skeleton. Ann Biomed Eng 31, 1314–1326.

Tait JF, Frieden C (1982). Polymerization-induced changes in the fluorescence of actin labeled with iodoacetamidotetramethylrhodamine. Arch Biochem Biophys 216, 133–141.

Taverna RD, Langdon RG (1973). Reversible association of cytochalasin B with the human erythrocyte membrane. Inhibition of glucose transport and the stoichiometry of cytochalasin binding. Biochim Biophys Acta 323, 207–219.

Tuvia S, Levin S, Bitler A, Korenstein R (1998). Mechanical fluctuations of the membrane-skeleton are dependent on F-actin ATPase in human erythrocytes. J Cell Biol 141, 1551–1561.

Tuvia S, Levin S, Korenstein R (1992). Oxygenation-deoxygenation cycle of erythrocytes modulates submicron cell membrane fluctuations. Biophys J 63, 599–602.

Vera C, Skelton R, Bossens F, Sung LA (2005). 3-D nanomechanics of an erythrocyte junctional complex in equibiaxial and anisotropic deformations. Ann Biomed Eng 33, 1387–1404.

Wang J, Fan Y, Dube DK, Sanger JM, Sanger JW (2014). Jasplakinolide reduces actin and tropomyosin dynamics during myofibrillogenesis. Cytoskeleton (Hoboken) 71, 513–529.

Wang F, Herzmark P, Weiner OD, Srinivasan S, Servant G, Bourne HR (2002). Lipid products of PI(3)Ks maintain persistent cell polarity and directed motility in neutrophils. Nat Cell Biol 4, 513–518.

Waterman-Storer CM (2001). Microtubule/organelle motility assays. Curr Protoc Cell Biol Chapter 13, Unit 13.11.

Yoon YZ, Hong H, Brown A, Kim DC, Kang DJ, Lew VL, Cicuta P (2009). Flickering analysis of erythrocyte mechanical properties: dependence on oxygenation level, cell shape, and hydration level. Biophys J 97, 1606–1615.